Atmospheric Inversion Strength over Polar Oceans in Winter Regulated by Sea Ice

Tamlin M. Pavelsky[1,2,*], Julien Boé[1], Alex Hall[1], Eric J. Fetzer[3]

[1]Dept. of Atmospheric and Oceanic Sciences, University of California Los Angeles Box 951565, Los Angeles, CA 90095

[2]Dept. of Geological Sciences, University of North Carolina, CB 3315, Chapel Hill, NC 27599

[3]Jet Propulsion Laboratory, California Institute of Technology, M/S 169-237, 4800 Oak Grove Drive, Pasadena, CA 91109

[*]Corresponding Author: pavelsky@ucla.edu, Phone: 919-962-4239, Fax: 919-966-4519

Keywords: Temperature Inversion, Sea Ice, Arctic, Antarctic, AIRS

Abstract

Low-level temperature inversions are a common feature of the wintertime troposphere in the Arctic and Antarctic. Inversion strength plays an important role in regulating atmospheric processes including air pollution, ozone destruction, cloud formation, and negative longwave feedback mechanisms that shape polar climate response to anthropogenic forcing. The Atmospheric Infrared Sounder (AIRS) instrument provides reliable measures of spatial patterns in mean wintertime inversion strength when compared with available radiosonde observations and reanalysis products. Here, we examine the influence of sea ice concentration on inversion strength in the Arctic and Antarctic. Correlation of inversion strength with mean annual sea ice concentration, likely a surrogate for the effective thermal conductivity of the wintertime ice pack, yields strong, linear relationships in the Arctic (r=0.88) and Antarctic (r=0.86). We find a substantially greater influence of sea ice concentration on surface air temperature than temperature at 850 hPa, lending credence to the idea that sea ice controls inversion strength through modulation of surface heat fluxes. As such, declines in sea ice in either hemisphere may imply weaker mean inversions in the future. Comparison of mean inversion strength in AIRS and global climate models (GCMs) suggests that most GCMs poorly characterize mean inversion strength at high latitudes.

1. Introduction

Low-level temperature inversions have long been recognized as a pervasive feature of the Arctic (Wexler 1936; Vowinkel and Orvig 1970; Curry 1996) and Antarctic (Phillpot and Zillman 1970; Connolley 1996) atmospheres in winters. They arise from multiple sources including warm air advection and subsidence, though a deficit in net surface radiation is the most common cause (Serreze et al. 1992; Liu et al. 2006). Inversion strength and depth regulate processes central to polar climate, including the depth of the atmospheric mixed layer and transport of heat and moisture from leads and polynyas (Andreas and Murphy 1986). In both hemispheres, photochemical destruction of ozone during the polar sunrise in springtime is partially controlled by inversion strength (Oltmans et al. 1989; Barrie et al. 1988; Wessel et al. 1998). The strength of katabatic winds over the Antarctic continent and coastal regions is strongly influenced by the depth and strength of the atmospheric inversion over Antarctica (Connolley 1996). In addition, temperature changes associated with the Southern Annular Mode (SAM) and other patterns of interannual atmospheric variability are controlled by spatial variations in mean inversion strength, with stronger mean inversions associated with greater SAM influence on surface air temperature (van den Broeke and van Lipzig 2004; van den Broeke 1998).

In the Arctic, the vertical structure of the atmosphere plays a strong role in regulating high concentrations of pollutants near the top of the inversion layer (Bridgeman et al. 1989) and cloud formation, with diminished inversion strength resulting in decreased low-level and increased midlevel cloudiness (Schweiger et al. 2008). Moreover, inversion strength plays a central role in negative longwave radiation feedback mechanisms that influence the extent of temperature and sea ice changes in the Arctic in response to anthropogenic warming (Boé et al. in press). Accurate characterization of these mechanisms is of particular importance in global climate models (GCMs) used to predict future climate. Boé et al. (in press) suggest that models used in the Intergovernmental Panel on Climate Change (IPCC) Fourth Assessment Report (AR4) generally overestimate mean inversion strength in the Arctic and, as a result, the strength of the negative longwave feedback.

Radiosonde observations show that wintertime temperature inversion maxima at both poles occur over land areas, especially Siberia and portions of the Canadian Archipelago in the north and East Antarctica in the south, where a cold land surface combines with favorable topography and generally high atmospheric pressure to produce extremely stable atmospheric conditions (Phillpot and Zillman 1970; Curry 1996; Serreze et al. 1992). Direct observations over the Arctic Ocean and adjacent seas are uncommon, with temporally discontinuous data from drift stations and aircraft providing limited coverage (Vowinkel and Orvig 1970; Serreze et al. 1992). These limited observations suggest that wintertime inversion strength over the Arctic Ocean can be as high as 15 K, with mean inversion depth ranging from 1000-1500 m (Serreze et al. 1992; Curry et al. 1996). Radiosonde observations over ice-covered oceans around Antarctica are almost entirely absent, resulting in little knowledge of the spatial and temporal structure of inversions from *in situ* methods. Recently, methods using remotely sensed observations have been developed to track inversion strength and depth. Empirical relationships between radiosonde-derived inversion strength and Moderate Resolution Imaging Spectroradiometer (MODIS) images have been used to examine spatial variations in inversion strength for individual days in the Arctic and Antarctic (Liu and Key 2003). Inversion climatologies have been constructed at both poles using observations from the High Resolution Infrared Sounder (HIRS) instrument (Liu et al. 2006). Gettelman et al. (2006) demonstrate that the Atmospheric Infrared Sounder (AIRS) can successfully reconstruct relative humidity inversions over the Antarctic continent. The AIRS satellite instrument is the main source of atmospheric data for this study.

The remote sensing and *in situ* studies noted above reveal that inversion strength exhibits considerable spatial and temporal variability over Arctic and Antarctic oceans. The goal of this paper is to determine the principal control on this variability. Recent research suggests a link between sea ice concentration (SIC) and inversion strength (Vavrus et al. 2000; Schweiger et al. 2008; Francis et al. 2009). However, no comprehensive examination of the relationship between SIC and inversion strength has been presented to date. Spatial variability in SIC may impact mean inversion strength by regulating heat exchange between the ocean and atmosphere. Specifically, we hypothesize that high SICs are associated with reduced loss of oceanic heat to the atmosphere and hence low surface air temperatures and that the effect of high SICs dissipates with altitude, resulting in stronger inversions over high-ice areas. Here, we compare measurements of wintertime temperature inversion strength from AIRS over Arctic and Antarctic oceans with satellite-derived sea ice concentrations. The results demonstrate that sea ice concentration is a principal determinant of inversion strength over polar oceans in both hemispheres.

2. Data and Methods

2.1 Inversion Strength Measurements from Satellite, Radiosonde, and Reanalysis

The AIRS experiment, included on the NASA Aqua satellite mission, comprises co-boresited microwave and infrared nadir viewing instruments (Aumann et al. 2003). Observed radiances are inverted to yield about 200,000 daily profiles of atmospheric temperature, water vapor and trace gases, along with cloud and surface properties (Chahine et al. 2006). The validity of the temperature profiles for a wide range of geophysical states has been established by Divakarla et al. (2006). Fetzer et al. (2004) used radiosondes and model reanalyses to demonstrate that AIRS can resolve near-surface temperature inversions for warm conditions west of the subtropical continents. Gettelman et al. (2006) show that AIRS can obtain accurate temperature and water vapor retrievals in nominal 1-2 km resolution over the cold Antarctic Plateau. Here, AIRS temperatures are used to measure wintertime temperature inversion strength over the Arctic, which we define as north of 64N, and the Antarctic (south of 64S).

Past studies of high-latitude temperature inversions have used varied definitions of inversion strength, including the difference between surface air temperature and maximum air temperature below the 700 hPa level (Liu et al. 2006) and the difference in air temperature between the lowest pressure level showing a temperature increase and the next layer where temperature decreases (Serreze et al. 1992). Because AIRS has limited vertical resolution in the lower troposphere, such flexible definitions of inversion strength are impractical in this case. Instead, we use fixed definitions of inversion strength. Differences in definition may cause absolute values of inversion strength in this study to vary from previous studies. In the northern hemisphere, we use the temperature difference between the 1000 hPa and 850 hPa pressure levels for the winter months of December, January, and February (DJF). We choose these two levels because the mean inversion height of 1000-1500 m over the Arctic Ocean found in previous studies (Curry 1996; Serreze et al. 1992) approximates the mean elevation of the 850 hPa pressure level (~1500 m). Wintertime surface pressure climatology over the much of the Southern Ocean is less than 1000 hPa, so in the southern hemisphere we instead use the AIRS estimate of surface air temperature (SAT) for June, July, and August (JJA). SAT is linearly interpolated from the AIRS vertical temperature profile and, as a result, may exhibit systematic biases relative to radiosonde observations. However, spatial patterns in SAT in both hemispheres closely match those at 1000 and 925 hPa. Because the principal goals of this study relate to spatial and temporal variability in inversion strength rather than the precise inversion value, results are largely insensitive to systematic bias associated with the choice of pressure level for the inversion base.

To ensure accuracy, AIRS inversion strength is compared with radiosonde-derived inversions at 29 locations in the terrestrial Arctic and Subarctic. Observations were extracted from the NOAA Integrated Global Radiosonde Archive (IGRA) (http://www.ncdc.noaa.gov/oa/climate/igra/index.php). Observations used here are located north of 64N and provide daily temperature observations at 1000 and 850 hPa over at least half of the wintertime AIRS observation period (December 2002-February 2008).

While radiosonde observations provide a very reliable measure of inversion strength, spatial coverage is limited, with no long-term observations available over Arctic or Antarctic oceans. Bromwich and Wang (2005) found that inversion strength computed from the NCEP and ERA-40 reanalysis products closely match radiosonde-derived wintertime inversion strength at selected locations over the Arctic Ocean. Here, correlation of spatial patterns in wintertime inversion strength derived from AIRS with both NCEP and ERA-40 provides some additional measure of the reliability of the AIRS dataset beyond isolated radiosonde locations. These reanalysis products assimilate few observations in the Arctic (and even fewer in the Antarctic) and are not sufficiently reliable to use as validations of the AIRS product (Kistler et al. 2001; Uppala et al. 2005). Still, AIRS and the two reanalysis products are independent, and strong correspondence among them would lend added confidence to the accuracy of each. The NCEP reanalysis is available from 1948 to present, and below we will compare AIRS inversions with (a) the long-term inversion strength climatology and (b) mean inversion strength over the AIRS observation period (2002-2008). The AIRS record does not overlap the ERA-40 reanalysis period (1957-2002), so in this case we will compare climatological AIRS inversions only with the long-term ERA-40 climatology.

2.2 Sea Ice Concentration Data

Maps of sea ice concentration (**Figure 1cd, Figure 2bc**) are extracted from the Defense Meteorology Satellite Program Special Sensor Microwave Imager (SSM/I) Monthly Polar Gridded Sea Ice Concentrations, available from the National Snow and Ice Data Center (http://nsidc.org/data/nsidc-0002.html; Comiso et al. 1990). This product provides a measure of fractional sea ice cover over the Arctic and Antarctic on 25 km polar stereographic grids and has been used extensively to examine trends in sea ice extent (e.g. Serreze et al. 2007). We directly compare spatial patterns in mean wintertime (DJF in the Arctic, JJA in the Antarctic) inversion strength and two SIC metrics derived from this product (described Section 3) to assess the direction and strength of sea ice/inversion relationships.

3. Quality of AIRS data

Results presented in **Figures 1a** and **1b** indicate that spatial variations in AIRS-derived inversions in the Arctic and Subarctic land areas closely match those from radiosondes, with a Pearson's correlation coefficient of $r=0.93$ and a regression line slope of $s=1.08$. AIRS consistently underestimates inversion strength relative to radiosonde observations by an average of 2.05 K for the 29 stations used here. Comprehensive global comparisons by Divakarla et al. (2006) reveals that height-dependent bias in AIRS temperature retrieval is largest in high-latitude inland and coastal areas, precisely those locations where we compare AIRS and radiosonde inversions. Bias over high-latitude oceans is small by comparison (Divakarla et al. 2006), suggesting that the systematic bias seen in **Figure 1b** is likely not representative of the Arctic Ocean as a whole. Radiosonde observations are extremely scarce in the Antarctic, and we do not attempt to provide separate validation for the southern hemisphere.

Spatial patterns in mean AIRS wintertime inversion over the entire Arctic north of 64N closely match those from the NCEP reanalysis product over the AIRS study period (r=0.80, **Table 1**). Correlations of AIRS inversions with spatial patterns in the long-term NCEP (r=0.76) and ERA-40 (r=0.75) inversion climatologies over the entire Arctic are also strong. AIRS inversions exhibit even higher correlations with reanalyses over Arctic oceans (r>0.90 in all cases). Mean wintertime inversion strengths over the entire northern hemisphere study area are very similar when calculated using AIRS, ERA-40, and the 2002-2008 NCEP period (**Table 1**). In contrast, dataset means exhibit somewhat more spread over the ocean, with AIRS showing the lowest mean inversion strength. The long-term NCEP climatology shows somewhat higher mean inversion strengths in both cases, though this may be due to temporal inhomogeneities in the reanalysis and limited observations assimilated into NCEP in the Arctic, leading to a product that is principally model-derived (Kistler et al. 2001).

In the Antarctic, it is not possible to compute inversion strengths over much of the continent with the definition used here because ice sheet elevation in many areas is greater than the 850 hPa pressure level. As such, we examine southern hemisphere inversion strengths only over the ocean (**Figure 2, Table 2**). Spatial correlations between

AIRS and reanalysis products are relatively high over the oceans in all cases, though somewhat lower than in the Arctic. This may reflect the almost complete lack of observations assimilated by the reanalyses over Antarctic oceans. Mean inversion strengths diverge substantially between AIRS and ERA-40 (low mean inversions) and the two NCEP time periods (high inversions). In fact, mean NCEP inversions are stronger over Antarctic oceans than in the Arctic, which seems incongruous given the greater eddy kinetic energy in the atmosphere and lower mean annual sea ice concentration values in the Antarctic (Peixoto and Oort, 1992). Since the NCEP dataset is strongly influenced by model output over Antarctic oceans, we suggest that the mean AIRS inversion values are likely more reliable. If AIRS is correct then the average inversion strength over Antarctic oceans south of 64S is, in fact, slightly negative. This results from the inclusion of both areas with weakly positive inversions and areas with a strongly negative atmospheric temperature gradient. The latter occur where wintertime and annual sea ice concentrations are low. AIRS is the only gridded dataset (of those examined here) based everywhere on observational data, and spatial patterns in AIRS inversions are both internally consistent and a close match with patterns in reanalysis and radiosonde inversions. As such, we have high confidence in results based on spatial and temporal patterns in the AIRS dataset.

4. Sea Ice – Inversion Relationship

Spatial comparison of mean wintertime SIC with mean wintertime inversion strength yields very high and statistically significant positive correlations for both the Arctic

(**Figure 3a**, r=0.78) and Antarctic (**Figure 4a**, r=0.63). The relationship is nonlinear in each case, however, with a substantial increase in the range of inversion strength values as SIC approaches 100%. If we instead compare wintertime inversion strength with average annual SIC (**Figures 3b, 4b**), still stronger and more linear relationships emerge in both hemispheres (r=0.88 in the Arctic, 0.86 in the Antarctic). This improvement arises largely from the behavior of locations with high wintertime SIC. In the Arctic, examination of only those areas where wintertime SIC >90% (shown in red) reveals low correlations in **Figure 3a** (r=0.22) but a statistically significant correlation in **Figure 3b** (r=0.71). A similar result is evident for high SIC areas in the Antarctic in **Figures 4a** (r=0.43) and **4b** (r=0.77).

To explain these differences, we suggest that annual SIC is a surrogate for wintertime ice thickness, particularly in areas where wintertime SIC is nearly saturated. Areas with high wintertime but lower annual SIC will likely contain more extensive sub-areas of thin, first-year ice in the winter than will areas with high ice concentration in all seasons. As heat transport through first-year ice is substantially greater than through multiyear ice (Lindsay and Rothrock 1994; Schramm et al. 1997), pixels containing extensive first-year ice in the winter will have higher surface air temperatures and weaker inversions than other pixels with high wintertime ice concentrations. A comparison of **Figures 3c** and **3d** reveals that variations in Arctic SIC principally influence temperatures at the surface, as opposed to at 850 hPa, which supports this hypothesis. While both 1000 hPa and 850 hPa temperatures are strongly anticorrelated with annual SIC, the 1000 hPa regression slope (s=-0.24 K/%SIC) is more than twice the 850 hPa slope (s=-0.10 K/%SIC). The same phenomenon is apparent in the Antarctic (**Figures 4a** and **4b**), though the surface air temperature regression slope is somewhat lower (s=-0.18 K/%SIC) than in the Arctic. This slight contrast may relate to several differences between the hemispheres including stronger eddy activity in the Southern Ocean and differences in physical characteristics of the ice packs.

Though the linear ice extent/inversion strength relationships evident in the Arctic (**Figure 3b**) and Antarctic (**Figure 4b**) are quite strong, some scatter remains. One cause of this scatter is likely that annual SIC is an imperfect metric of the bulk thermal conductivity of the ice pack. A map of residuals from the best-fit linear regression in the Arctic (not shown) reveals spatially coherent patterns unrelated to ice concentration. In the northern hemisphere, the linear regression model overestimates inversion strength east of Greenland and underestimates it in the Canadian archipelago and over the Laptev and East Siberian seas. These geographic patterns may be associated with large-scale atmospheric circulation and topographic influence, which past studies have shown to affect inversion strength (Vowinkel and Orvig 1970; Curry 1996). Residual patterns are less spatially coherent in the southern hemisphere (not shown), though inversion strength in the Weddell Sea is slightly underestimated by the best-fit regression equation.

5. Discussion and Conclusions

Based on the strong statistical relationship between SIC and mean wintertime inversion strength presented in **Figures 3** and **4**, sea ice is a principal driver of spatial variability in inversion strength in the high latitude oceans of both hemispheres. The hypothesis that the influence of SIC on temperature is greatest at the surface and dissipates with elevation is borne out by the substantially greater regression slopes at the surface compared with 850 hPa and the positive correlations at both levels. There are several physical mechanisms that may help explain the SIC-inversion relationships observed here. In areas with low and moderate SIC, greater heat flux from open water compared to sea ice is likely the governing factor. Where ice cover is more continuous, the presence of leads and polynyas plays a similar role. In addition, the percolation of seawater directly through brine channels in ice occurs more frequently where ice cover is thin (Lytle and Ackley, 1996). As a result, those areas with high wintertime SIC that contain large areas of thin, first-year ice will likely experience greater heat flux from the ocean to the atmosphere than will areas of thick, multi-year ice. Sensible heat flux is also greater through first-year ice cover, which may reinforce this disparity (Lindsay and Rothrock 1994; Schramm et al. 1997). The influence of the latter two mechanisms is likely highest in areas where wintertime SIC is greatest, highlighted in **Figures 3** and **4** in red. Given that a higher proportion of first-year ice is likely in areas with lower mean annual SIC values, it is unsurprising that a linear relationship between mean annual SIC and mean wintertime inversion strength exists, even where wintertime SIC is nearly 100%.

It is somewhat unexpected that SIC/inversion relationships are so similar in the two hemispheres given differences in atmospheric circulation patterns and ice growth and decay mechanisms. This similarity suggests that the mechanisms by which sea ice drives inversion strength are similar in both polar oceans. However, we also find that mean inversion strength over Antarctic oceans is somewhat lower than in the Arctic. This result likely stems from several differences between the hemispheres, including the southern hemisphere's lower overall mean annual SIC (SH: 62%, NH: 74%) and the extremely limited area of thick, multiyear ice in the Antarctic. Substantially greater eddy activity over ice-covered areas in the Antarctic than in the Arctic (Peixoto and Oort 1992) would also lower atmospheric stability.

Rapid changes in SIC and thickness recently observed over the Arctic Ocean (Serreze et al. 2007; Giles et al. 2008; Armstrong et al. 2003) suggest that mean wintertime inversion strength may be decreasing over time. The AIRS satellite record is of insufficient length to capture long-term trends, and trend analysis using reanalysis products is unreliable. Comparison of monthly area-averaged SIC with inversion strengths for December, January and February 2002-2008 (n=18) yields a correlation coefficient of r=0.71, suggesting that a positive temporal relationship may exist (**Figure 5a**). In the southern hemisphere (**Figure 5b**), we perform a similar analysis using June, July, and August 2003-2008 SICs and inversion strengths and find a similarly strong positive correlation (r=0.62). A weaker mean inversion would have several important implications for polar climate in the future. High concentrations of atmospheric pollutants near the top of the Arctic inversion layer will likely decline as stability of the lower troposphere decreases. Schweiger et al. (2008) also suggest that low-level cloudiness may decrease while midlevel cloudiness may increase in most areas of the Arctic, which would influence atmospheric heat and moisture transport.

Inversion strength is often poorly represented in global climate simulations. We compare area-averaged mean wintertime inversion strength over Arctic oceans (**Figure 6a**) in 17 general circulation models included in the Coupled Model Intercomparison Project 3 (CMIP3) with values from satellite and reanalysis datasets presented here. We find a bias towards unrealistically high inversion strength in 15 of the 17 models compared with mean AIRS inversion strength. If we instead use mean NCEP inversion strength since 1948, the strongest inversions of all observational products examined here, 8 models still overestimate inversion strength. Given the documented relation between climatological inversion strength and the strength of the longwave feedback parameter in the Arctic (Boé et al., in press), it is likely that most models inaccurately represent the strength of the negative longwave feedback parameter and thus underestimate the response of Arctic climate to anthropogenic forcing. The picture is less clear in the southern hemisphere (**Figure 6b**), where some models show very strong mean wintertime inversions, while others show no inversions. Still, 10 of the 17 models examined differ by at least 2 K from the mean AIRS inversion value. Results shown in this study suggest that to correct these errors it is worthwhile examining simulations of the sea ice-inversion relationship.

Acknowledgements

This research was funded by the National Science Foundation under grant ARC-0714083. Opinions, findings, or recommendations expressed here are those of the authors and do not necessarily reflect NSF views. We acknowledge the modeling groups, the Program for Climate Model Diagnosis and Intercomparison (PCMDI) and the WCRP's Working Group in Coupled Modeling (WGCM) for their roles in making available the WCRP

CMIP3 multi-model dataset. Support for this dataset is provided by the Office of Science, U.S. Department of Energy. ECMWF ERA-40 data used in this study have been obtained from the ECMWF data server.

References

Andreas EL, Murphy B (1986) Bulk transfer coefficients for heat and momentum over leads and polynyas. J Phys Oceanogr 16:1875-1883.

Armstrong, AE, Tremblay LB, and Mysak LA (2003) A data-model intercomparison study of Arctic sea ice variability. Climate Dynamics 20:465–476. doi.10.1007/s00382-002-0284-2

Aumann, HH et al. (2003), AIRS/AMSU/HSB on the Aqua mission: design, science objectives, data products and processing system. IEEE Trans Geosci and Remote Sensing, 41:253-264.

Barrie LA, Bottenheim JW, Schnell RC, Crutzen RC, Rasmussen RA (1988) Ozone destruction and photochemical reactions at polar sunrise in the lower Arctic atmosphere. Nature 334:1875-1883.

Boé J, Hall AD, Qu X (In Press), Current GCMs' unrealistic negative feedback in the Arctic, J Climate.

Bridgman HA, Schnell RC, Kahl JD, Herbert GA, Joranger E (1989) A major haze event near Point Barrow, Alaska: Analysis of probable source regions and transport pathways. Atmos Environ 23:2537-2549.

Bromwich DH, Wang SH (2005) Evaluation of the NCEP–NCAR and ECMWF 15- and 40-Yr Reanalyses using rawinsonde data from two independent arctic field experiments. Mon Wea Rev 133:3562-3578.

Chahine MT et al. (2006) The Atmospheric Infrared Sounder (AIRS): improving weather forecasting and providing new insights into climate. Bull. Amer. Meteor. Soc. 87:891–894. doi:10.1175/BAMS-87-7-891.

Comiso J (1990, updated 2005) DMSP SSM/I daily and monthly polar gridded sea ice concentrations, 2002-2008. Edited by Maslanik J, Stroeve J. Boulder, Colorado USA: National Snow and Ice Data Center, http://nsidc.org/data/nsidc-0002.html, accessed 07 Jul 2009.

Connolley WM (1996) The Antarctic temperature inversion, Int J Climatol 16:1333-1342.

Curry JA, Rossow WB, Randall D, and Schramm JL (1996) Overview of Arctic cloud and radiation characteristics, J Climate 9:1731-1764.

Divakarla, MG, Barnet CD, Goldberg MD, McMillin LM, Maddy E, Wolf W, Zhou L, Liu X (2006) Validation of Atmospheric Infrared Sounder temperature and water vapor retrievals with matched radiosonde measurements and forecasts. J Geophys Res 111:D09S15. doi:10.1029/2005JD006116

Fetzer EJ, Teixeira J, Olsen E, Fishbein E (2004) Satellite remote sounding of atmospheric boundary layer temperature inversions over the subtropical eastern Pacific. Geophys Res Lett, 31:L17102. doi:10.1029/2004GL020174.

Francis JA, Chan W, Leathers DJ, Miller JR, and Veron DR (2009) Winter northern hemisphere weather patterns remember summer Arctic sea-ice extent. Geophys Res Lett 36:L07503. doi:10.1029/2009GL037274

Gettelman A, Walden VP, Miloshevich LM, Roth WL, and Halter B (2006) Relative humidity over Antarctica from radiosondes, satellites, and a general circulation model. J Geophys Res 111:D09S13. doi:10.1029/2005JD006636

Giles KA, Laxon SW, and Ridout AL (2008) Circumpolar thinning of Arctic sea ice following the 2007 record ice extent minimum. Geophys Res Lett 45:L22502. doi:10.1029/2008GL035710

Kistler R, Kalnay E, Collins W et al (2001) The NCEP/NCAR 50-year reanalysis: Monthly means CD-ROM and documentation. Bull. Amer. Meteor. Soc. 82:247-268.

Lindsay RW, Rothrock DA (1994) Arctic sea ice temperature from AVHRR. J. Climate, 7:174-183.

Liu Y, Key JR, Schweiger A, Francis J (2006) Characteristics of satellite-derived clear-sky atmospheric temperature inversion strength in the Arctic, 1980-96. J Climate 19:4902-4913.

Liu Y, Key JR (2003) Detection and analysis of clear sky, low-level atmospheric temperature inversions with MODIS. J Atmos Oceanic Technol 20:1727-1737.

Lytle VI, Ackley SF (1996) Heat flux through sea ice in the western Weddell Sea: Convective and conductive transfer processes. J Geophys Res 101(C4):8853-8868.

Maykut GA (1978) Energy exchange over young sea ice in the central Arctic. J Geophys Res, 83(C7):3646-3658.

Meehl GA et al (2007) Global Climate Projections in Climate Change 2007: The physical Science Basis: contributions of Working Group I to the Fourth Assessment Report of the Intergovernmental Panel on Climate Change. Cambridge University Press, Cambridge, UK and New York.

Oltmans SJ, Schnell RC, Sheridan PJ, Peterson RE, Li SM, Winchester JW, Tans PP, Sturges WT, Kahl JD, Barrie LA (1989) Seasonal surface ozone and filterable bromine relationship in the high Arctic. Atmos Environ 23:2431-2441.

Peixoto JP, Oort AH (1992) The Physics of Climate. American Institute of Physics, New York.

Phillpot HR, Zillman JW (1970) The surface temperature invesion over the Antarctic Continent. J Geophys Res 75(21):4161-4169.

Schweiger AJ, Lindsay RW, Varvus S, Francis JA (2008) Relationships between Arctic sea ice and clouds during autumn. J Climate 21:4799-4810.

Serreze MC, Holland MM, Stroeve J (2007) Perspectives on the Arctic's shrinking sea-ice. Science 5818:1533-1536. doi:10.1126/science.1139426

Serreze MC, Kahl JD, Schnell RC (1992) Low-level temperature inversions of the Eurasian Arctic and comparisons with Soviet drifting station data. J. Climate 5:615-629.

Schramm JL, Holland MM, Curry JA, Ebert EE (1997) Modeling the thermodynamics of a sea ice thickness distribution 1. Sensitivity to ice thickness resolution. J Geophys Res 102(C10): 23079-23091.

Tebaldi C, Knutti R (2007) The use of the multi-model ensemble in probabilistic climate projections. Phil Trans R Soc A 365: 2053-2075.

Uppala SM et al (2005) The ERA-40 Reanalysis, Quarterly Journal of the Royal Meteorological Society 131:2961–3012. doi: 10.1256/qj.04.176

Van den Broeke MR (1998) The semiannual oscillation and Antarctic Climate. Part 1: influence on near surface temperatures (1957-79). Antarctic Science, 10(2):175-183.

Van den Broeke MR, van Lipzig NMP (2004) Changes in Antarctic temperature, wind and precipitation response to the Antarctic Oscillation. Ann Glaciol 39:119-127.

Vavrus S, Gallimore R, Liu Z (2000) A mixed-flux equilibrium asynchronous coupling scheme for accelerating convergence in ocean-atmosphere models, Climate Dynamics 16:821-831. doi: 10.1007/s003820000082.

Vowinkel E, Orvig S (1970) The climate of the North Polar Basin. In Orvig S (ed) World Survey of Climatology, vol 14: Climates of the Polar Regions. Elsevier, pp 129-226.

Wessel S, Aoki S, Winkler P, Weller R, Herber A, Gernandt H, Schrems O (1998) Tropospheric ozone depletion in polar regions: A comparison of observations in the Arctic and Antarctic. Tellus 50B:34-50.

Tables

Dataset	Time Period	Mean Inversion (K)	Correlation with AIRS	Mean Inversion (Ocean) (K)	Correlation with AIRS (Ocean)
AIRS	2002-2008	1.81	1.00	-0.42	1.00
NCEP	2002-2008	1.64	0.80	0.64	0.90
NCEP	1948-2008	2.77	0.76	2.21	0.92
ERA-40	1957-2002	1.63	0.75	1.23	0.95

Table 1: Mean inversion strength in satellite and reanalysis datasets over the entire Arctic north of 64N and only over the ocean.

Dataset	Time Period	Mean Inversion (Ocean) (K)	Correlation with AIRS (Ocean)
AIRS	2002-2008	-1.37	1.00
NCEP	2002-2008	2.82	0.72
NCEP	1948-2008	4.08	0.72
ERA-40	1957-2002	-0.16	0.86

Table 2: Mean inversion strength in satellite and reanalysis datasets over Antarctic oceans south of 64S.

Figures

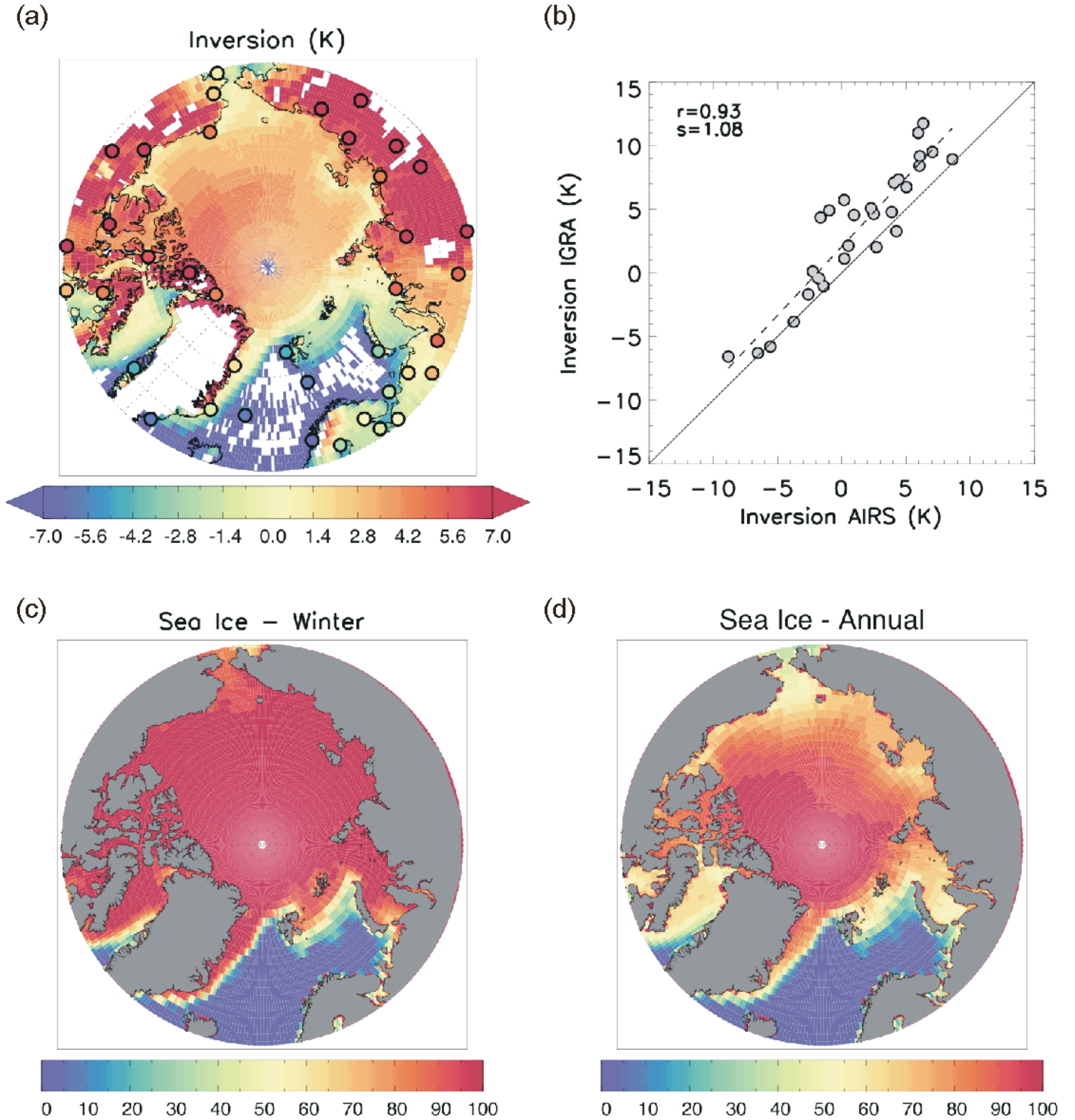

Figure 1: (a) mean DJF AIRS inversion strength from December 2002- February 2008, with mean DJF inversion strength from radiosondes over the same period superimposed. (b) scatterplot of mean AIRS inversion strength and radiosonde inversion strength at points shown in (a). Linear correlation coefficient of 0.93 is statistically significant at $p<0.01$. (c) Mean wintertime (DJF) sea ice concentration (SIC) from SSM/I satellite data from September 2002-February 2008, (d) Mean annual SIC from SSM/I satellite data from September 2002-February 2008.

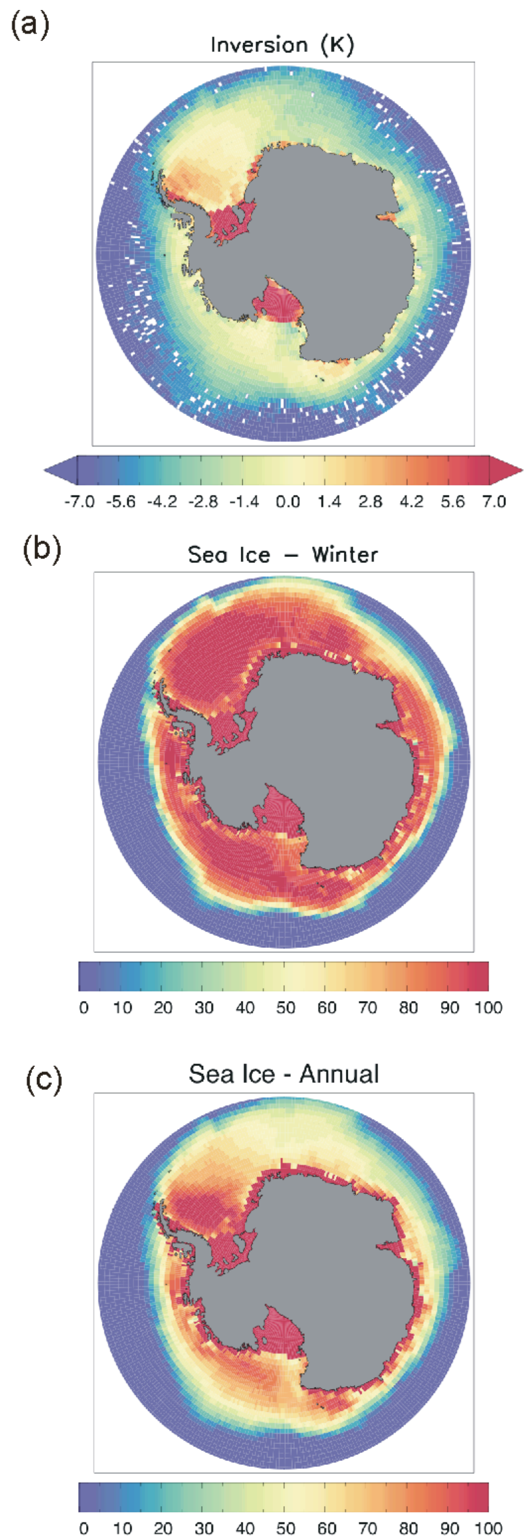

Figure 2: (a) mean wintertime (JJA) AIRS inversion strength from June 2003- August 2008 for the Antarctic. (b) Mean JJA sea ice concentration (SIC) from SSM/I satellite data from September 2002-February 2008, (d) Mean annual SIC from SSM/I satellite data from September 2002-February 2008.

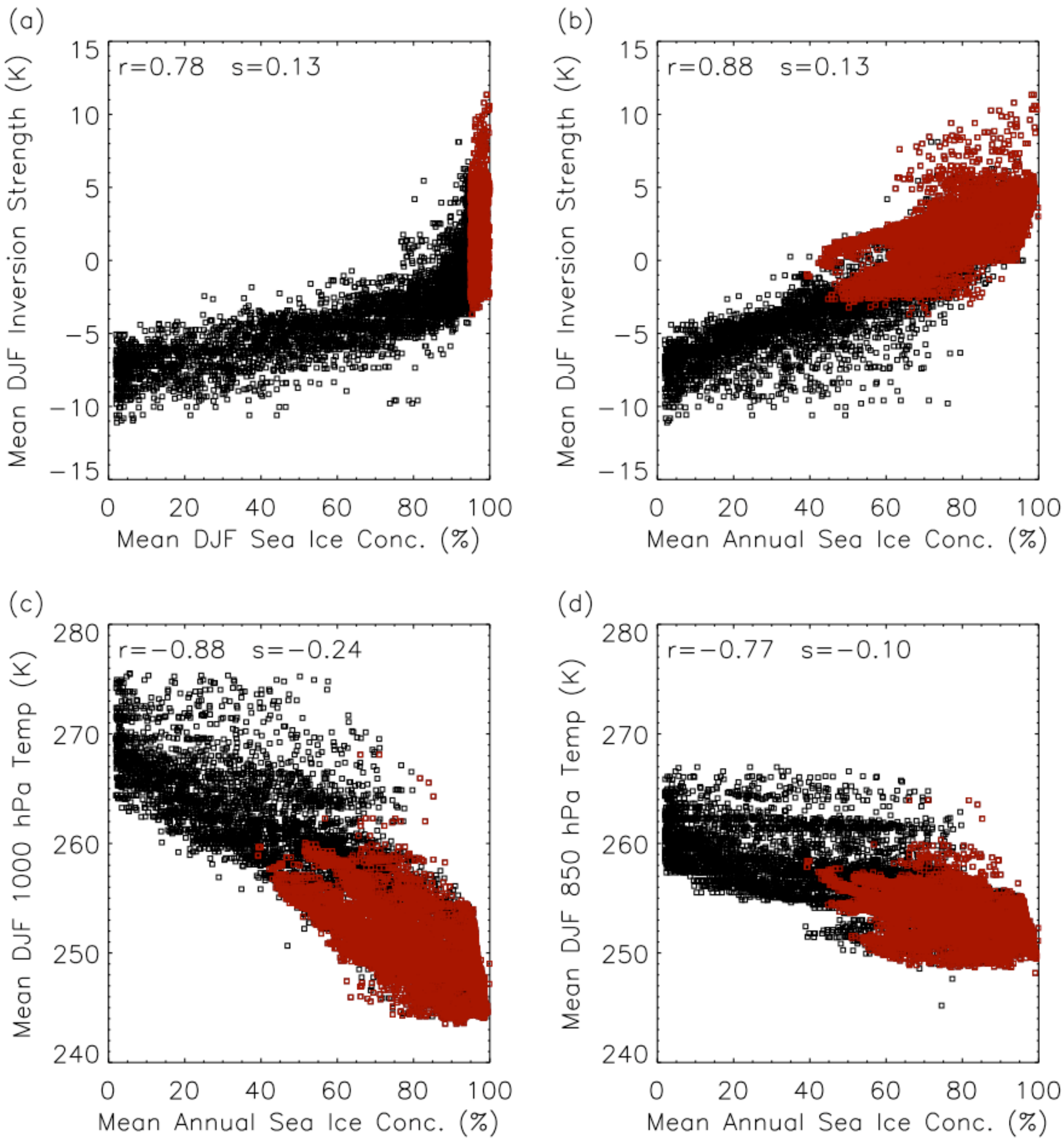

Figure 3: Scatterplots for Arctic north of 64N between (a) mean AIRS DJF inversion strength and mean DJF sea ice concentration (SIC) from SSM/I, (b) mean AIRS DJF inversion strength and mean annual SIC, (c) mean AIRS DJF 1000 hPa temperature and mean annual SIC, and (d) mean AIRS DJF 850 hPa temperature and mean annual SIC. Points in red are those points with DJF SIC > 90%, which show little covariance with inversions strength in (a) but are strongly correlated with inversion strength in (b) and (c).

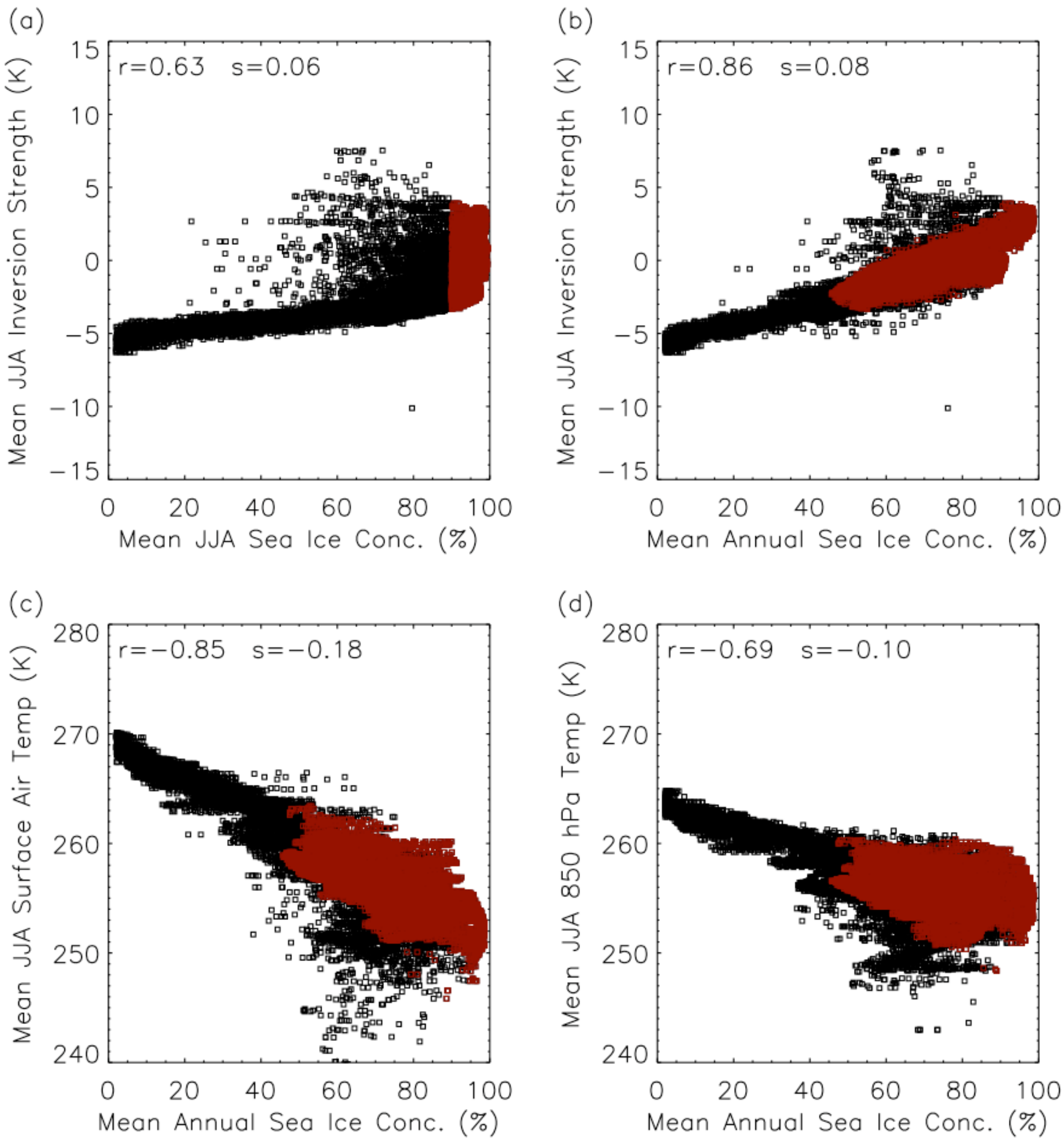

Figure 4: Scatterplots for Antarctic south of 64S between (a) mean AIRS JJA inversion strength and mean JJA sea ice concentration (SIC) from SSM/I, (b) mean AIRS JJA inversion strength and mean annual SIC, (c) mean AIRS JJA surface air temperature temperature and mean annual SIC, and (d) mean AIRS JJA 850 hPa temperature and mean annual SIC. Points in red are those points with JJA SIC > 90%, which show little covariance with inversions strength in (a) but are strongly correlated with inversion strength in (b) and (c).

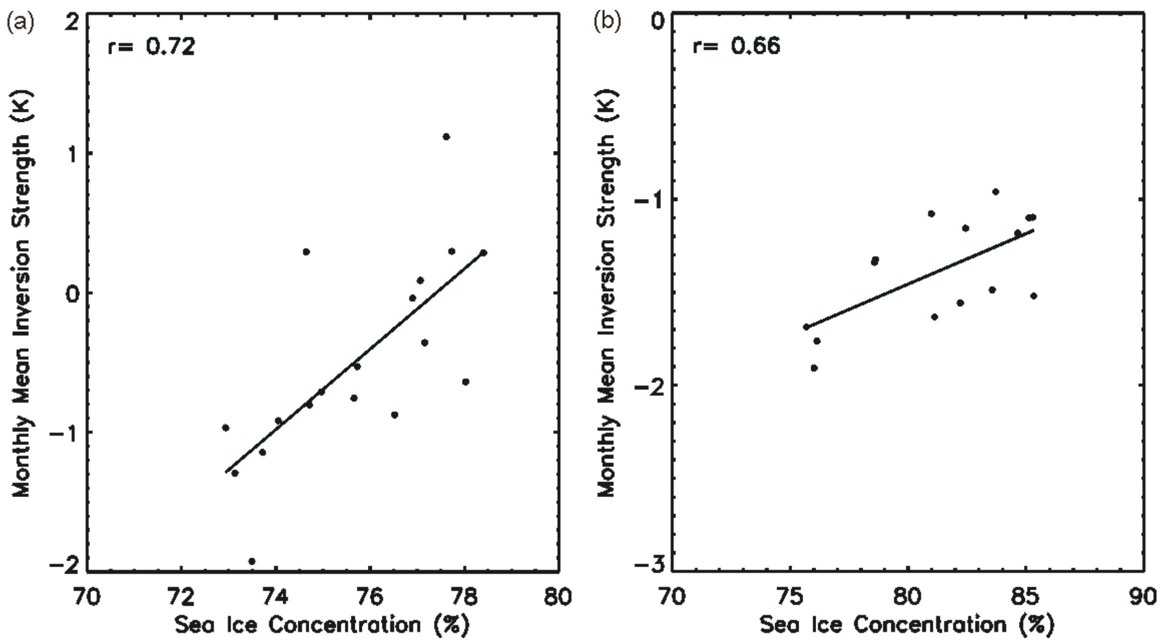

Figure 5: Scatterplots between wintertime monthly area-averaged inversion strength and sea ice concentration for the Arctic (a) and Antarctic (b). Each point represents one month (DJF 2002-2008 in (a), JJA 2003-2008 in (b)).

(a)

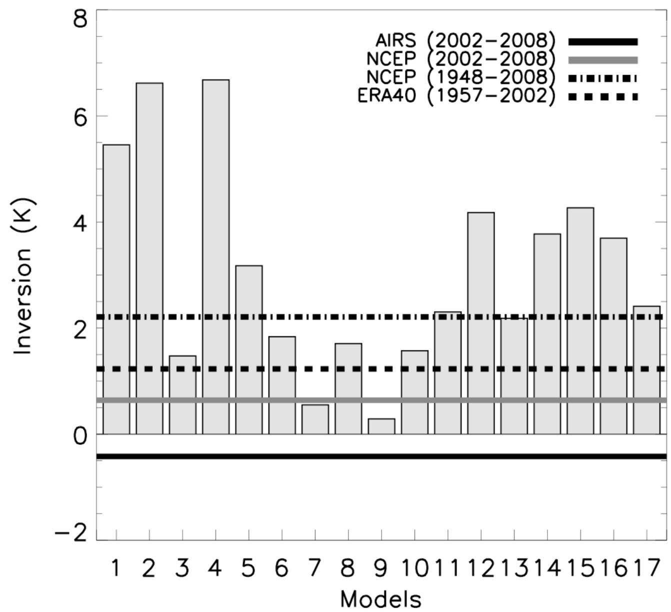

(b)

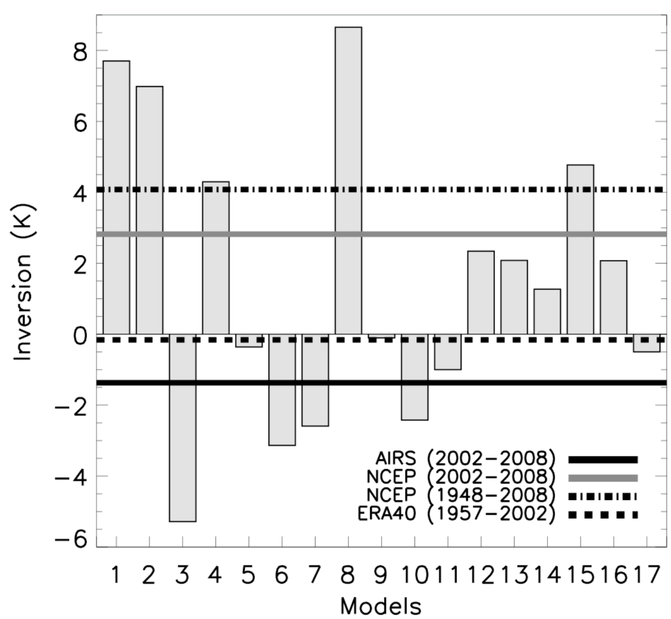

Figure 6: Climatological strength of the inversion in the 1960-1999 period as simulated by17 CMIP3 models (Meehl et al., 2007) over (a) Arctic oceans and (b) Antarctic oceans. Solid and dashed lines indicated mean inversion strength from NCEP and ERA-40 reanalysis products and from AIRS satellite data. All the available models are used: (1) cccma_cgcm3_1, (2) cccma_cgcm3_1_t63, (3) cnrm_cm3, (4) csiro_mk3_0, (5) gfdl_cm2_0, (6) gfdl_cm2_1, (7) giss_model_e_r, (8) inmcm3_0, (9) ipsl_cm4, (10) miroc3_2_medres, (11) mpi_echam5, (12) mri_cgcm2_3_2a, (13) ncar_ccsm3_0, (14) ncar_pcm1, (15) ukmo_hadgem1, (16) ukmo_hadcm3, (17) bccr_bcm2_0